Dalton Transactions

ROYAL SOCIETY OF CHEMISTRY

PAPER

View Article Online
View Journal | View Issue

Cite this: *Dalton Trans.*, 2021, **50**, 2393

Coordination chemistry of the bench-stable tris-2-pyridyl pnictogen ligands [E(6-Me-2-py)$_3$] (E = As, As═O, Sb)†

Alex J. Plajer,*[a] Daniel Crusius, [a] Rajesh B. Jethwa, [a] Álvaro García-Romero,[b] Andrew D. Bond, [a] Raúl García-Rodríguez *[b] and Dominic S. Wright *[a]

Received 29th October 2020,
Accepted 26th November 2020

DOI: 10.1039/d0dt03732j

rsc.li/dalton

Tripodal ligands with main group bridgehead units are well established in coordination chemistry and single-site organometallic catalysis. Although a large number of tris(2-pyridyl) main group ligands [E(2-py)$_3$] (E = main group element, 2-py = 2-pyridyl) spanning across the whole p-block are now synthetically acessible, only limited work has been done on the coordination chemistry on the tris(2-pyridyl) group 15 ligands for the heavier elements (As, Sb). In the current study we investigate the coordination chemistry of the ligand family E(6-Me-2-py)$_3$ (E = As, Sb) and of the As(v) ligand O═As(6-Me-2-py)$_3$. The air- and mositure-stability of all of these main group ligands makes them especially attractive in future catalytic applications.

1. Introduction

Tripodal ligands are very common as facially coordinating 6-electron donor ligands in single-site homogeneous transition metal catalysis and biomimetic chemistry.[1,2] One of the most prominent types of tripodal ligands employed are tris-pyrazolyl borates (Fig. 1a), as a result of the ease by which the steric and electronic properties of these ligands can be tuned by substituents on the pyrazolyl rings.[3–5] Although not as well developed as a ligand class, tris-pyridyl ligands [E(2-py′)$_3$] (Fig. 1b), containing a range of main group element bridgehead atoms (E), have also emerged.[6,7] Changing the bridgehead atoms in these ligands not only allows the incorporation of a further donor centre, but also provides an additional tool for altering ligand bite and donor strength. Earlier work in this area had concentrated on ligands containing non-metal bridgehead atoms (*e.g.*, CR, COR, CH, N, P, P═O).[8]

Our focus has been on the most metallic p-block elements (Fig. 1, lower panel).[9–13] Coordination of metal-based ligands of this type to a range of main group and transition metal atoms provides a simple approach to the assembly of heterometallic complexes. In addition, introducing electropositive metal atoms also has a large effect on the charge distribution within the ligand frameworks and their reactivity. For example, aluminates of type **A** (Fig. 1, lower panel) are useful 2-pyridyl transfer reagents which are stable at room temperature.[14,15] Their acid–base reactivity with alcohols makes them useful as reagents in the quantitative determination of enantiomeric excess of mixtures of chiral alcohols.[16] We also showed recently that the increase in Lewis acidity moving down group 15 in the pnictogen ligands **B** (E = As, Sb, Bi) (Fig. 1, lower panel) can drastically alter the 6-methyl-2-pyridyl ligand coordination mode and can be used to change their net donor

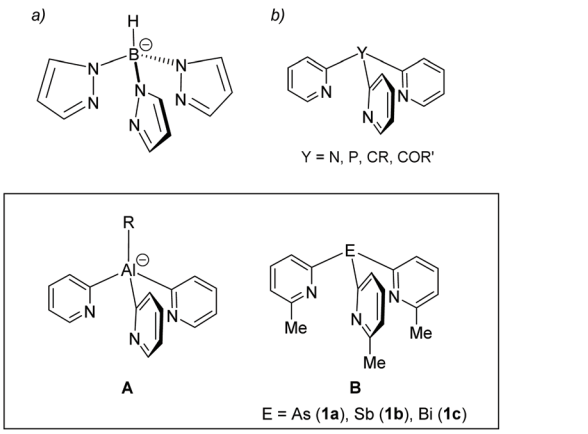

Fig. 1 (a) The parent tris-pyrazolyl-borate anion and (b) the family of neutral unsubstituted tris (2-pyridyl) ligand containing non-metal bridgeheads. The inset shows two examples of metal-based analogues.

[a]*Chemistry Department, Cambridge University, Lensfield Road, Cambridge, CB2 1EW, UK*
[b]*GIR MIOMeT-IU Cinquima-Química Inorgánica, Facultad de Ciencias, Campus Miguel, Delibes, Universidad de Valladolid, 47011 Valladolid, Spain.*
E-mail: raul.garcia.rodriguez@uva.es

†Electronic supplementary information (ESI) available: NMR spectroscopic and X-ray characterisation. CCDC 2039592–2039603 and 2039862. For ESI and crystallographic data in CIF or other electronic format see DOI: 10.1039/d0dt03732j

character systematically.[17] However, this previous work only explored Cu(I) complexes of these heavier group 15 ligands.

The stability of the series of group 15 ligands [E(6-Me-2-py)$_3$] (**B**) under ambient conditions, unlike the majority of metal-based ligands of this type, makes them particularly attractive, for example, as far as their development in the area of catalysis is concerned. Although the coordination chemistry of the parent, unsubstituted [E(2-py)$_3$] ligands has been investigated extensively for the lighter elements (E = N and P), there have been almost no structural studies of tris-2-pyridyl ligands containing the heavier group 15 elements and the only such studies of the Sb and Bi ligands were reported by us recently (and, as previously noted, were limited to coordination of Cu^{I}).[8,17] In this paper we explore the coordination chemistry of the group 15 tris-2-pyridyl ligands [E(6-Me-2-py)$_3$] (E = As, Sb) and, in the case of the As^{III} ligand, the effects of oxidising the bridgehead atom in the series of As^{V} ligands [X = As(6-Me-2-py)$_3$] (X = O, S, Se). This work provides a basis for understanding the principal coordination modes for the ligands containing the heavier elements and how these compare to the N- and P-analogues.

2. Results and discussion

As we noted in our initial paper in this area,[17] the incorporation of the 6-Me group into the 2-pyridyl units of the heavier group 15 ligands [E(6-Me-2-py)$_3$] [E = As (**1a**), Sb (**1b**)] leads to a significant increase in their stability compared to unsubstituted 2-py groups. The parent As^{III}-bridged tris-pyridyl ligand [As(2-py)$_3$] has been prepared previously,[18,19] and ligands **1a** and **1b** are readily obtained in good yields (60–64%) using the reactions of lithiate 6-Me-2Li-py with ECl_3 in THF (Scheme 1).[17] Contrary to our expectations, during the initial stages of the current work we found that, due to the stabilising effect the 6-Me substituents in the 2-pyridyl framework, both ligands are indefinitely stable in air under ambient conditions.

Since we had shown previously that changes in the Lewis acidity of the group 15 element had a major effect on the donor strength and coordination mode of the ligands, we were also interested to assess the potential effects of oxidation of the As^{III} atom of **1a** on charge distribution and coordination preference. The arsenic oxide ligand [O=As(6-Me-2-py)$_3$] (**1a**-O) is obtained in 72% yield by the oxidation of **1a** with H_2O_2 in THF, after removal of the solvent under vacuum. This new ligand was characterised using ^{1}H, ^{13}C NMR, IR, UV-Vis and elemental analysis, prior to obtaining its single-crystal X-ray structure. Comparison of the IR spectrum with that of **1a** allowed the assignment of the As=O stretching frequency in **1a**-O at 902 cm^{-1} (Ph_3As=O 880 cm^{-1}).[20] Oxidation of the As bridgehead in **1a** has a large effect on the solubility of the ligands. While **1a** and **1a**-O are indefinitely stable under ambient conditions in air, **1a**-O is also soluble and stable in water as a solvent (as shown by ^{1}H NMR spectroscopy). The solid-state structure of **1a**-O shows that incorporation of the O-atom at the bridgehead position, not unexpectedly, pushes the 6-Me substituents away due to repulsion with the As=O bond, consistent with a simple VSEPR model (Fig. 2, left). The orientation of the 6-Me-2-py groups in **1a**-O is different from that in the parent ligand **1a** (reported previously[17]) in which the 6-Me-groups are all orientated (upwards) towards the As^{III} atom (Fig. 2, right). Oxidation also has the effect of reducing the bridgehead As–C_α bond lengths by approximately 0.04 Å and increasing the bridgehead C–As–C angles compared to the parent ligand **1a** (from 92.3(2) in **1a** to 102.4(1)–106.3(1)° in **1a**-O). The latter can be seen as a direct consequence of the more sterically congested orientation of the 6-Me groups in **1a**-O, but is also in-line with VSEPR arguments concerning the effect of the increase in the electronegativity of the As centre on C–As/C–As bonding-pair repulsion.

Coordination studies of **1a**, **1a**-O and **1b** were undertaken with a range of transition metal salts. The results are summarized in Fig. 3. The new complexes [(**1a**-O) Cu(CH$_3$CN)]PF$_6$ (**2**), [Ag@Ag$_x$(**1a**)$_4$](O$_2$CCF$_3$)$_{1+x}$ (**3**), [(**1a**-O)Ag(O$_2$CCF$_3$)] (**4**), [(**1a**)CoBr$_2$] (**5**), [(**1a**-O)$_2$CoBr](CoBr$_3$NCCH$_3$) (**6**), [(**1a**)NiBr$_2$] (**7**), [(**1a**-O)NiBr$_2$] (**8**), [(**1a**)(Cymene)RuCl$_2$] (**9a**) and [(**1b**)(Cymene)RuCl$_2$] (**9b**), and [(**1a**)$_2$PtCl$_2$] (**10a**) and [(**1b**)$_2$PtCl$_2$] (**10b**) have been synthesized and characterised by ^{1}H and ^{13}C{^{1}H} NMR (where applicable), IR, UV-Vis and elemental analysis. Their single-crystal X-ray structures were also obtained (see Fig. 3 for their structural formulae).

The 1 : 1 stoichiometric reaction of [Cu(CH$_3$CN)$_4$]PF$_6$ with **1a**-O in CH$_3$CN at room temperature yields the complex [(**1a**-O)Cu(CH$_3$CN)]PF$_6$ (**2**) in 31% isolated yield after crystallization from the concentrated reaction mixture at −14 °C. The ^{1}H

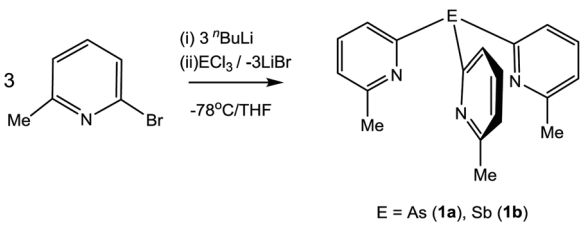

Scheme 1 Synthesis of the heavier group 15 ligand **1a** and **1b**.

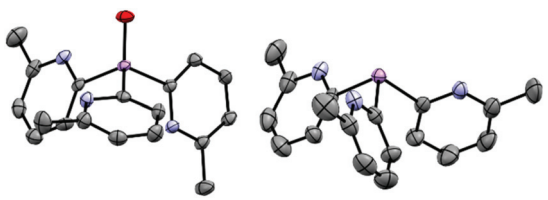

Fig. 2 (Left) molecular structure of the ligand **1a**-O, showing displacement ellipsoids at 50% probability, with H-atoms omitted. Selected bond lengths (Å) and angles (°): As=O 1.641(2), As–$C_{pyridyl}$ range 1.939(3)–1.943(3), $C_{pyridyl}$–As–$C_{pyridyl}$ range 105.9(1)–106.3(1), As–$C_{pyridyl}$–N range 113.8(2)–114.4(2). Colour key, As (pink), nitrogen (blue). (right) X-ray structure of the ligand **1a**. All 6-Me groups and N-atoms of the pyridyl ring units are orientated ("upwards") towards the arsenic bridgehead. X-ray data taken from reference.[17]

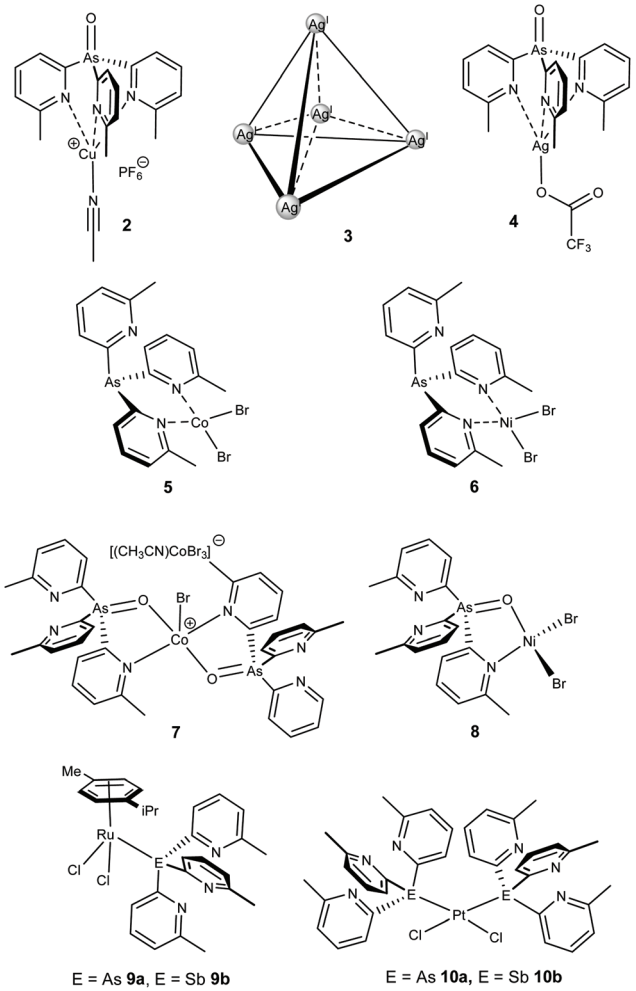

Fig. 3 Transition metal complexes of ligand **1a**, **1a**-O and **1b** obtained in the current work. The face-capping ligands have been omitted form the structure of **3** for clarity.

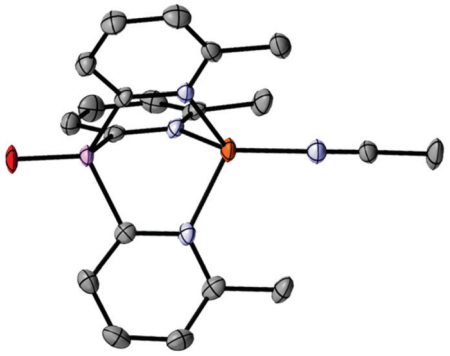

Fig. 4 Molecular structure of the cation of **2**. H-atoms and the PF_6^- anion omitted for clarity, with displacement ellipsoids at 50% probability. Selected bond lengths (Å) and angles (°): As=O 1.635(2), As–$C_{pyridyl}$ range 1.927(3)–1.930(3), Cu–$N_{pyridyl}$ range 2.081(3)–2.136(2), Cu–NCMe 1.950(3), $C_{pyridyl}$–As–$C_{pyridyl}$ range 105.6(1)–105.6(9), As–$C_{pyridyl}$–N range 116.8(2)–117.0(2), $N_{pyridyl}$–Cu–$N_{pyridyl}$ range 98.69(7)–100.6(1). Colour key, Cu (orange), As (pink), N (blue), O (red).

NMR spectrum at room temperature shows a single pyridyl environment, but with very broad resonances that sharpen upon cooling to −30 °C. This is in contrast to the previously reported $CuPF_6$ complex of the un-oxidised ligand **1a**, [(**1a**)Cu$(CH_3CN)]PF_6$, for which sharp resonances are observed even at room temperature and might suggest that a fluxional process is occurring in **2** in which the coordination of a pyridyl-N atom to Cu^I is exchanging with As=O coordination. N,O-coordination is observed later in this study in a number of other complexes of **1a**-O. In the solid state, **2** adopts an ion-separated structure containing $[\{O{=}As(6\text{-Me-2-py})_3\}CuCH_3CN]^+$ cations, in which the Cu^I atom is chelated by all three of the pyridyl-N atoms, and PF_6^- anions (Fig. 4). This metal coordination mode is commonplace for tris-2-pyridyl ligands and is the same as that found in the previously reported $CuPF_6$ complexes of **1a** and **1b**.[17] The only noticeable differences between the cations [(**1a**) $Cu(CH_3CN)]^+$ and [(**1a**-O) $Cu(CH_3CN)]^+$ stem from the larger bridgehead bite angles in **1a**-O, the bridgehead C–As–C angles for **1a**-O being *ca.* 5° greater than in the [(**1a**-O) $Cu(CH_3CN)]^+$ cation, resulting in an associated large increase in the $N_{pyridyl}$–Cu–$N_{pyridyl}$ angles (by *ca.* 15–23°) compared to the [(**1a**)$Cu(CH_3CN)]^+$ cation.

The UV-Vis absorption spectrum of **2** shows two distinct bands at 265 nm and 333 nm which can be assigned to a ligand π–π* transition and a Cu^I-to-ligand charge transfer transition (MLCT).[21–23] These values are similar to those observed in the previously reported As^{III} analogue [(**1a**)$Cu(CH_3CN)]PF_6$ (270 nm and 359 nm, respectively). While the π–π* transitions in [(**1a**)$Cu(CH_3CN)]PF_6$ and **2** are identical to that found in the ligands **1a** (269 nm) and **1a**-O (265 nm), respectively, the MLCT band shows a small blue shift comparing [(**1a**)Cu $(CH_3CN)]PF_6$ to **2**. This can be attributed to an increase in ligand-field strength, similar to conclusions made by Kodera *et al.* for the family of $[RC(6\text{-Me-2-py})_3]Cu(CH_3CN)]PF_6$ complexes (R = H, Me, Et).[24]

The 1 : 1 stoichiometric reaction of AgO_2CCF_3 with **1a** in CH_3CN at room temperature yields the cluster $[Ag@Ag_x(\mathbf{1a})_4](O_2CCF_3)_{1+x}$ (**3**) in an isolated crystalline yield of 21%, after layering the concentrated reaction mixture with Et_2O. The arrangement of **3** was established *via* single-crystal X-ray analysis (Fig. 5). The cationic cluster in **3** $[Ag@Ag_x(\mathbf{1a})_4]^{(1+x)+}$ has a very similar structural arrangement to the previously reported compound $[Ag@Ag_4(P(2\text{-py})_3)_4]^{5+}$,[25] which comprises an Ag-centred Ag_4 tetrahedral core, with four As^{III} ligands (**1a**) coordinating three Ag^+ cations over each face of the tetrahedron. Unlike $[Ag@Ag_4(P(2\text{-py})_3)_4]^{5+}$, however, in which the Ag^+ cations are also coordinated by PF_6^- anions or solvent molecules, the presence of the sterically-blocking 6-Me groups in **1a** prevents further coordination of the Ag centres, so that they remain three coordinate (trigonal planar).

The structure of **3** is probably viewed most appropriately as an $[Ag(As(6\text{-Me-2-py})_3)_4]^+$ cation, involving tetrahedral coordination of the central Ag^+, with the outer Ag^+ ions being captured by coordination to the pyridyl rings of the $As(6\text{-Me-2-py})_3$ ligands. The central $[Ag(As(6\text{-Me-2-py})_3)_4]^+$ core resembles the

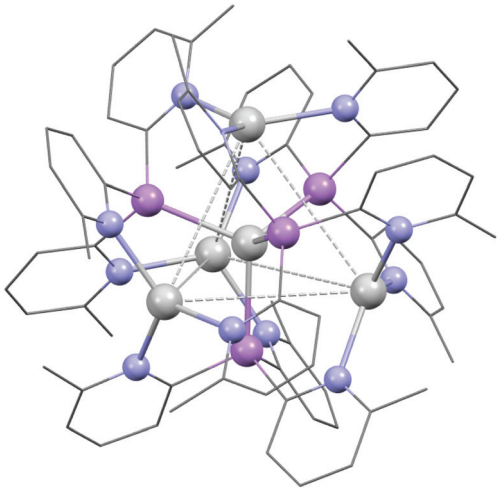

Fig. 5 Structure of the cluster compound $[\{Ag@Ag_x\{(6\text{-Me-2-py})_3\}As\}_4(CF_3COO)_{1+x}]$ (**3**), with CF_3COO^- and H atoms omitted for clarity. Colour key, Ag (white), As (pink), N (blue). The X-ray crystal structure of **3** suggests partial site occupancy of the outer Ag^+ atoms, and the exact nature of $[Ag@Ag_x(\mathbf{1a})_4]^{(1+x)+}$ remains uncertain.

well-established tetrahedral ion $[Ag(AsPh_3)_4]^+$. Supporting this, the Ag–As bond length in $[Ag(AsPh_3)_4]^+$ span the range 2.645–2.668 Å (mean 2.653 Å), compared to the range 2.594(2)–2.691(2) Å seen in **3**.[26] The comparison to $[Ag(AsPh_3)_4]^+$ indicates that the $[Ag(As(6\text{-Me-2-py})_3)_4]^+$ cation should exist independently from further coordination of the outer Ag^+ ions. The ion therefore has the potential to span the range from +1 to +5, depending on the extent of Ag^+ coordination in the pyridyl binding sites. This is consistent with the observation of partial site occupancy of the Ag^+ ions within the tetrahedral unit of **3** (see ESI†). However, it is difficult to verify this hypothesis from the X-ray data, since the trifluoroacetate counterions required for charge balance are also poorly resolved. ^1H and ^{13}C NMR spectra at room temperature in MeCN solution show multiple, broad pyridyl environments. Since the analogous cluster $[Ag@Ag_4(P(2\text{-py})_3)_4]^{5+}$ is reported to stay intact in MeCN,[25] this may support the suggestion of variable coordination within an intact $[Ag@Ag_x(\mathbf{1a})_4]^{(1+x)+}$ cluster, but it may also indicate that $[Ag@Ag_x(\mathbf{1a})_4]^{(1+x)+}$ disassembles in solution. At the present time, the similarity to $[Ag@Ag_4(P(2\text{-py})_3)_4]^{5+}$ is established, but the exact nature of $[Ag@Ag_x(\mathbf{1a})_4]^{(1+x)+}$ remains uncertain.

The reaction of AgO_2CCF_3 with **1a**-O in CH_3CN at room temperature gives the crystalline complex $[(\mathbf{1a}\text{-O})Ag(O_2CCF_3)]$ (**4**) in 21% isolated yield after crystallization from the concentrated reaction mixture at −14 °C. The local C_3-symmetric (*N*,*N*,*N*) coordination of Ag^I is apparent from the ^1H NMR spectrum for **4** which shows only one sharp 6-Me-2-py environment. The single-crystal X-ray structure is that of an ion-paired complex in which the $O_2CCF_3^-$ anion also coordinates the metal centre (Fig. 6). The structure of **4** resembles the previously reported Ag^I complex $[\{Ag\{(2\text{-py})_3P{=}O\}(PPh_3)\}BF_4]$.[27] In both cases, the presence of the P/As=O substituent precludes the ligand bonding mode present in the clusters $[Ag@Ag_4(P(2\text{-py})_3)_4]$ and **3**.

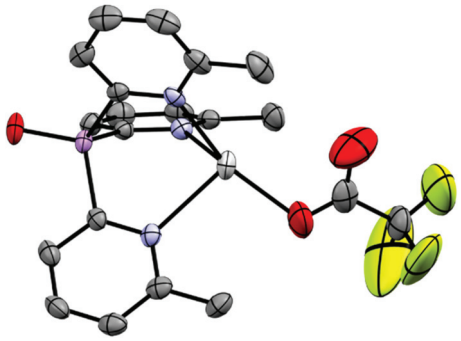

Fig. 6 Molecular structure of **4**, H-atoms and a second crystallographically independent molecule are omitted for clarity. Displacement ellipsoids are drawn at the 50% probability level. Selected bond lengths (Å) and angles (°) (range over both independent molecules): As=O 1.640(3), As–$C_{pyridyl}$ range 1.932(5)–1.942(5), Ag–$N_{pyridyl}$ range 2.313(4)–2.465(4), Ag–O 2.274(4)-2.32(3), $C_{pyridyl}$–As–$C_{pyridyl}$ range 106.3(2)–109.0(2), As–$C_{pyridyl}$–N range 117.2(3)–118.8(3), $N_{pyridyl}$–Ag–$N_{pyridyl}$ range 87.2(1)–94.6(1). Colour key, Ag (white), As (pink), N (blue), O (red), F (yellow).

The 1 : 1 stoichiometric reactions of $CoBr_2$ and $NiBr_2$ with **1a** and subsequent crystallization from the concentrated reaction mixtures at −14 °C give the corresponding 1 : 1 complexes $[(\mathbf{1a})NiBr_2]$ (**5**) (27% yield) and $[(\mathbf{1a})CoBr_2]$ (**6**) (22% yield), respectively. The solid-state structures of both show bidentate coordination of the metal centres using two of the three pyridyl-N atoms of **1a** (Fig. 7). The complexes are isostructural with each other and with the recently described complexes $[\{PhSi(6\text{-Me-2-py})_3\}CoCl_2]$ and $[\{PhSi(6\text{-Me-2-py})_3\}FeCl_2]$ containing the $PhSi(6\text{-Me-2-py})_3$ ligand.[28] Similarly to these com-

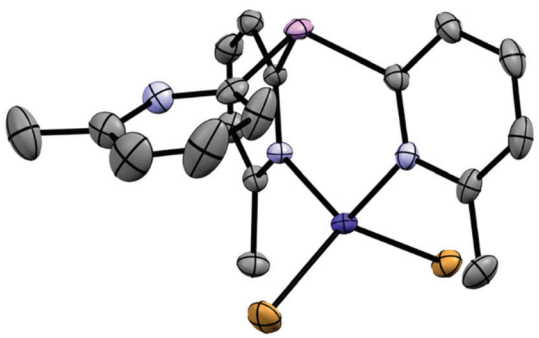

Fig. 7 Molecular structure of the complex $[(\mathbf{1a})CoBr_2]$ (**5**); $[(\mathbf{1a})NiBr_2]$ (**6**) is isostructural in the solid state. Displacement ellipsoids shown at 50% probability, with H atoms omitted for clarity. Selected bond lengths (Å) and angles (°): **5**, As–$C_{pyridyl}$ range 1.959(3)–1.965(3), Co–$N_{pyridyl}$ range 2.051(2)–2.052(2), Co–Br range 2.3684(6)–2.4080 (6), $C_{pyridyl}$–As–$C_{pyridyl}$ range 96.1(1)–104.2(1), As–$C_{pyridyl}$–N range 122.5(2)–123.8(2) (coordinating pyridyl groups), As–$C_{pyridyl}$–N 115.1(3) (non-coordinating pyridyl group), N–Co–N 109.1(1), Br–Co–Br 120.46(2). **6**, As–$C_{pyridyl}$ range 1.949(4)–1.975(5), Ni–$N_{pyridyl}$ range 2.018(3)–2.022(4), Ni–Br range 2.3484(8)–2.4029(8), $C_{pyridyl}$–As–$C_{pyridyl}$ range 96.0(2)–103.1(2), As–$C_{pyridyl}$–N range 122.3(3)–124.1(3) (coordinating pyridyl groups), As–$C_{pyridyl}$–N 115.3(3) (non-coordinating pyridyl group), N–Ni–N 107.1(1), Br–Ni–Br 130.23(3). Colour key, As (pink), N (light blue), Co (dark blue), Br (orange).

plexes, the adoption of a bidentate coordination mode is probably a consequence of the steric congestion of the 6-Me substituents, which prevents the coordination of smaller ions by all three of the pyridyl-N atoms. Although meaningful ^{1}H NMR studies of **5** proved impossible due to the paramagnetic nature of the complex, six distinct pyridyl resonances were observed for **6** at room temperature in MeCN, corresponding to the bonded and non-bonded 6-Me-2-py groups. The spectrum did not change with temperature, suggesting that the complex is intact in solution and that no fluxional interchange of 2-pyridyl ligand coordination is occurring. This is in contrast with the behaviour of the previously reported complexes [{PhSi(6-Me-2-py)$_3$}$CoCl_2$] and [{PhSi(6-Me-2-py)$_3$}$FeCl_2$] which are fluxional at room temperature.

Oxidation of the bridgehead atom of **1a** has a marked effect on the coordination preferences of ligand **1a**-O. The 1 : 1 stoichiometric reaction of $CoBr_2$ with **1a**-O in CH_3CN and subsequent crystallization from the concentrated reaction mixture at −14 °C yields blue crystals of [(**1a**-O)$_2$CoBr]($CoBr_3NCCH_3$) (**7**) in 74% yield. Surprisingly, the solid-state structure reveals an ion-separated arrangement containing [(**1a**-O)$_2$CoBr]$^+$ cations (Fig. 8) and [$CoBr_3NCCH_3$]$^-$ anions. Thus, overall, the complex has a 1 : 1 ratio of the ligand **1a** to $CoBr_2$. Within the [(**1a**-O)$_2$CoBr]$^+$ cations, the Co^{II} centre adopts a trigonal bipyramidal geometry in which two 2-pyridyl-N atoms of separate **1a**-O ligands bond at the axial positions. The Co^{II} cation is further coordinated in the equatorial plane by the bridgehead O-atoms of the ligands and by a Br$^-$ ion. The anion (which is not shown in Fig. 8) has a tetrahedral Co^{II} centre that is bonded to three Br$^-$ anions and a MeCN molecule. The paramagnetic ^{1}H NMR spectrum of **7** at room temperature in MeCN shows two sets of pyridyl resonances, indicating that the solid-state structure is maintained in solution.

The same N,O-coordination mode as seen in **7** is also observed in the Ni^{II} complex [(**1a**-O)$NiBr_2$] (**8**), obtained from the reaction of $NiBr_2$ with **1a**-O in CH_3CN in low yield (2%). In the solid-state structure (Fig. 9), the Ni^{II} centre is chelated by the bridgehead-O and a pyridyl-N atom of the ligand **1a**-O and further bonded to two Br$^-$ anions, giving a distorted tetrahedral geometry at the metal centre. The formation of **7** and **8** highlight that bridgehead oxidation can drastically change the ligand character of tris-pyridyl arsine ligands. This switch in coordination character from all-N to N,O (*e.g.*, comparing the Co^{II} complexes **5** and **7**) is no doubt largely a consequence of the relative hardness or softness of the ligand modes with respect to the metal coordinated. However, there may also be a more subtle influence of the steric effect of the 6-Me-substution of the pyridyl groups in **1a**-O on the preference for N-chelation *versus* N,O-chelation. It is noteworthy in this regard that the closely related, unsubstituted P^V ligand [O=P(2-py)$_3$] (which has been studied extensively) has been observed to bond almost exclusively using its pyridyl-N atoms, the only example of N,O-chelation similar to that seen in **7** and **8** being seen in [$MoBr(CO)_2(CH_2CHCH_2)${O=P(2-py)$_3$}].[8,29]

Having probed the coordination preferences of the arsines **1a** and **1a**-O, we moved on to explore the Sb-bridged ligand **1b**. Attempted oxidation of the Sb atom with H_2O_2 resulted in complicated mixtures of products. This was not pursued further since a localised Sb=O bonding arrangements (analogous to **1a**-O) would in any case not be expected, on the basis of the low bond energy compared to Sb–O single bonds.[30] Attempts to coordinate harder transition metal ions with **1b** often lead to the formation of intractable mixtures, preventing further analysis. This appears to be due to the greater polarity

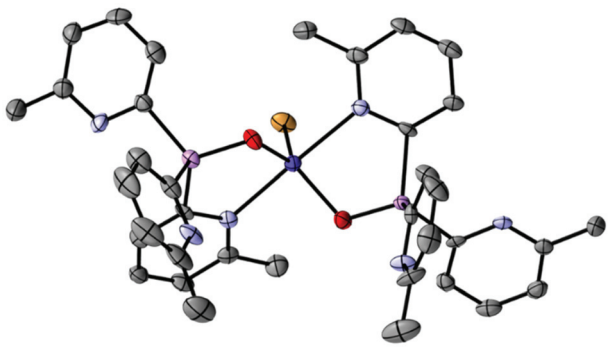

Fig. 8 Molecular structure of the cation of [(**1a**-O)$_2$CoBr]($CoBr_3NCCH_3$) (**7**), showing displacement ellipsoids at 50% probability, with H-atoms, lattice-bound CH_3CN and the counter-anion omitted for clarity. Selected bond lengths (Å) and angles (°): As–$C_{pyridyl}$ range 1.904(9)–1.940(9), As=O 1.672(6)–1.677(7), Co–$N_{pyridyl}$ range 2.240(8)–2.318(8), Co–Br 2.430(2), Co–O range 1.967(7)–1.971(7), $C_{pyridyl}$–As–$C_{pyridyl}$ range 106.3(4)–112.5(4), As–$C_{pyridyl}$–N range 107.7(8)–113.3(7), N–Co–N 177.4(3), O–Co–O 117.3(3), O–Co–Br range 121.3(2)–121.4(2). Colour key, As (pink), N (light blue), O (red), Co (dark blue), Br (orange).

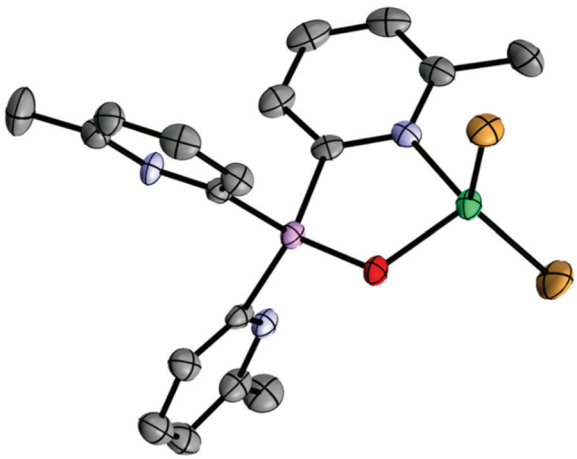

Fig. 9 Molecular structure of [(**1a**-O)$NiBr_2$] (**8**). Displacement ellipsoids are shown at 50% probability. H-atoms and lattice bound CH_2Cl_2 are omitted. Selected bond lengths (Å) and angles (°): As–$C_{pyridyl}$ range 1.908(7)–1.940(6), As=O 1.669(4), Ni–$N_{pyridyl}$ 2.021(6), Ni–Br range 2.342(1)–2.367(1), Ni–O 1.963(4), $C_{pyridyl}$–As–$C_{pyridyl}$ range 106.2(3)–112.3(3), As–$C_{pyridyl}$–N 111.(5) (coordinating pyridyl groups), As–$C_{pyridyl}$–N range 111.0(5)–114.3(5) (non-coordinating pyridyl group), O–Ni–N 93.0(2), Br–Ni–Br 134.01(6). Colour key, As (pink), N (light blue), Ni (light green), Br (orange).

of the bridgehead C–Sb bonds (which leads to 2-pyridyl transfer to the metal rather than coordination) and to greater sensitivity to hydrolysis by trace moisture present in the metal salts employed. Similar observations have been made by us recently in regard to the closely related Bi ligand [Bi(6-Me-2-py)$_3$].[31] For example, in the case of reaction of the Sb-ligand **1b** with $CoBr_2$ only the decomposition product [(6-Me-2-py)$_2$$CoBr_2$] could be isolated, as a result of transfer of the 6-Me-2-py groups to Co^{II} (see ESI†).

Reactions with softer transition metal centres were more successful, although under these circumstances metal coordination is observed to occur exclusively by the bridgehead Sb atom (reflecting the softness of the atoms involved). The room-temperature, 1 : 1 stoichiometric reactions of the arsenic ligand **1a** and the antimony ligand **1b** with [(Cymene)$RuCl_2$]$_2$ in CH_2Cl_2 result in quantitative formation of [(**1a**)(Cymene)$RuCl_2$] (**9a**) and [(**1b**)(Cymene)$RuCl_2$] (**9b**) within 5 minutes, as monitored *via in situ* ^{1}H NMR spectroscopy. Layering of the concentrated reaction mixtures with *n*-pentane yielded red crystalline **9a** and **9b** in 64% and 66% yield, respectively. The complexes have similar structures in the solid-state, in which the As and Sb bridgehead atoms coordinate the Ru^{II} centres (Fig. 10). There are only minor structural changes in the ligands upon coordination, with the pnictogen–ruthenium bond lengths increasing from 2.450(7) to 2.597(2) Å in line with the increase in the atomic radii of the heavier group 15 elements. The As–Ru and Sb–Ru bond lengths in both of the complexes are similar to those reported previously.[32,33] In both cases, room-temperature ^{1}H and ^{13}C NMR spectra in MeCN confirm that the local C_3 ligand symmetry is retained in solution, showing only one pyridyl environment. The aromatic cymene proton resonances in **9a** are found in the region δ 5.92–5.58 ppm whereas those in **9b** are in the range between δ 6.15–6.00 ppm. This indicates that the Sb atom in **9b** donates more electron density to the Ru atom in **9b** than the As atom does in **9a**, resulting in less π-donation in the former. This somewhat counterintuitive observation presumably reflects the relative softness of the Sb^{III} centre of **1b** in respect to the soft Ru^{II} centre.

Similar observations are made in regard to coordination of $PtCl_2$. Reactions of **1a** or **1b** with (benzonitrile)$_2$$PtCl_2$ in DCM for 5 minutes and subsequent layering of the concentrated reaction mixtures with *n*-pentane give the platinum complexes [(**1a**)$_2$$PtCl_2$] (**10a**) and [(**1b**)$_2$$PtCl_2$] (**10b**) as yellow crystals in 59% and 30% yields, respectively. The complexes are isostructural in the solid state (Fig. 11), in which the square-planar Pt^{II} atoms are bonded to two As- or Sb-atoms of **1a** or **1b**. The formation of the *cis* isomer in both cases is the result of the greater *trans* effect of the Cl ligands. Again, there are only minor changes in the structural parameters of the ligands compared to the isolated ligands themselves. The observed elongation of the pnictogen–Pt bonds going from **10a** to **10b** is consistent with the increase in the atomic radius of the group

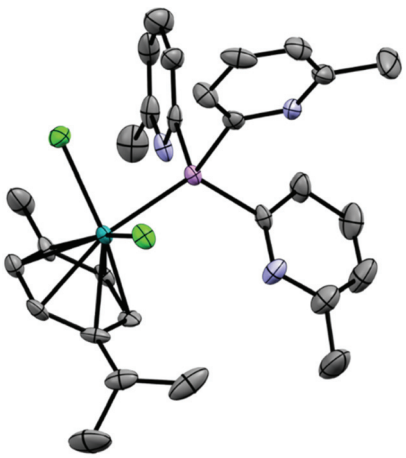

Fig. 10 Molecular structure of [(**1a**)(Cymene)$RuCl_2$] (**9a**); [(**1b**)(Cymene)$RuCl_2$] (**9b**) has a similar structure in the solid state, showing displacement ellipsoids at 50% probability; with H-atoms omitted. Selected bond lengths (Å) and angles (°): **9a**, As–$C_{pyridyl}$ range 1.953(4)–1.961(4), Ru–As 2.4509(4), Ru–Cl range 2.4232(9)–2.4233(9), Ru–C range 2.169(4)–2.222(3), $C_{pyridyl}$–As–$C_{pyridyl}$ range 99.9(2)–100.6(2), As–$C_{pyridyl}$–N range 113.3(3)–114.9(3), Ru–As–C range 112.2(1)–121.6(1), As–Ru–Cl range 83.86(3)–88.52(2), Cl–Ru–Cl 89.13(3). **10b**, Sb–$C_{pyridyl}$ range 2.144(3)–2.154(3), Ru–Sb 2.5976(3), Ru–Cl range 2.4061(9)–2.4115(8), Ru–C range 2.171(4)–2.208(4), $C_{pyridyl}$–Sb–$C_{pyridyl}$ range 99.4(1)–102.4(1), Sb–$C_{pyridyl}$–N range 113.1(2)–114.3(3), Ru–Sb–C range 113.4(1)–121.44(9), Sb–Ru–Cl range 84.44(2)–85.91(2), Cl–Ru–Cl 87.38(3). Colour key, As (pink), N (light blue), Ru (dark green), Cl (light green).

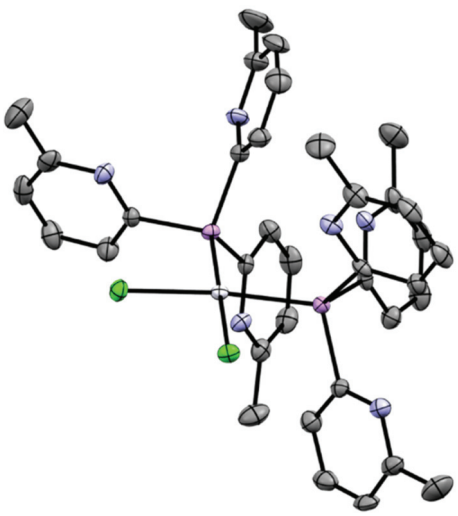

Fig. 11 Molecular structure of [(**1a**)$_2$$PtCl_2$] (**10a**); [(**1b**)$_2$$PtCl_2$] (**10b**) has a similar structure in the solid state, showing displacement ellipsoids at 50% probability; with H-atoms omitted. Selected bond lengths (Å) and angles (°): **10a**, As–$C_{pyridyl}$ range 1.948(4)–1.964(4), Pt–As range 2.3415(4)–2.3503(4), Pt–Cl range 2.3326(9)–2.3523(9), $C_{pyridyl}$–As–$C_{pyridyl}$ range 100.7(2)–109.4(2), As–$C_{pyridyl}$–N range 111.6(3)–119.5(3), Pt–As–C range 109.6(1)–121.4(1) As–Pt–Cl range 83.74(3)–89.81(3) (on same side), As–Pt–As 96.25(2), Cl–Pt–Cl 89.91(3). **10b**, Sb–$C_{pyridyl}$ range 2.126(8)–2.153(8), Pt–Sb range 2.4944(6)–2.4976(6), Pt–Cl range 2.336(2)–2.354(2), $C_{pyridyl}$–Sb–$C_{pyridyl}$ range 98.2(3)–109.1(3), Sb–$C_{pyridyl}$–N range 111.3(6)–114.8(6), Pt–Sb–C range 112.0(2)–121.2(2), Sb–Pt–Cl range 84.02(5)–88.49(6) (on same side), Sb–Pt–Sb 96.89(2), Cl–Pt–Cl 90.59(7). Colour key, As (pink), N (light blue), Pt (white), Cl (light green).

15 atoms involved (2.3415(6)–2.3501(5) in **10a** to 2.4945(6)–2.4977(7) in **10b**). The As–Pt and Sb–Pt bond lengths in both of the complexes are similar to those reported previously.[34,35]

Conclusions

In contrast to the more well studied phosphine ligands of the type [P(2-py′)$_3$] (where py′ is a substituted or unsubstituted pyridyl group) the 6-Me-2-pyridyl ligands **1a** and **1b** and the As (v) ligand **1a**-O are all indefinitely air- and moisture-stable, making them not only easy to make but also easy to use. Ligands **1a** and **1b** are robust enough to transfer to a range of transition metal centres. Oxidation of the bridgehead atom of the arsenic ligand **1a** can drastically change its coordination preferences, leading to a greater tendency for N,O-coordination involving the bridgehead O-atom and pyridyl groups. This tendency may well also be influenced by the presence of substituents on the 2-pyridyl groups in our case and can be compared to the related unsubstituted [O=P(2-py)] ligand, which is observed to bond almost exclusively using a chelating N-coordination mode. We are continuing our studies of the synthesis and coordination chemistry of main group pyridyl ligands of this type, with the aim of applying these ligands in catalysis and supramolecular chemistry.

Experimental section

General experimental techniques

Where indicated, experiments were carried out on a Schlenk-line under nitrogen atmosphere or with the aid of a N_2-filled glove box (Saffron type α). Although the ligands **1a**, **1b** and **1a**-O are all indefinitely air- and -moisture stable, anaerobic conditions were employed in reactions to avoid adventitious coordination of water to metal centres in the coordination compounds or potential metal oxidation during reactions. MeCN used for reactions was dried over CaH_2. *n*-Pentane, hexane and diethyl ether were dried over sodium or sodium/benzophenone. 6-Methyl-2-bromo-pyridine was distilled over CaH_2 and stored over 4 Å molecular sieves. If not specified other compounds were acquired from Aldrich Chemical Company. ^{1}H, ^{13}C {^{1}H} and ^{31}P{^{1}H} NMR spectra were recorded on a Bruker Avance 400 QNP or Bruker Avance 500 MHz cryo spectrometer. All spectra were recorded in $CDCl_3$, CD_2Cl_2 or CD_3CN, with $SiMe_4$ (^{1}H) or the solvent peaks as external and internal standards. Unambiguous assignments of NMR resonances were made on the basis of 2D NMR experiments (^{1}H–^{1}H COSY, ^{1}H–^{1}H NOESY, ^{1}H–^{13}C HMQC and ^{1}H–^{13}C HMBC). Fig. 12 shows the labelling scheme for NMR assignments used throughout the Experimental section. Elemental analysis was obtained using a PerkinElmer 240 elemental analyser.

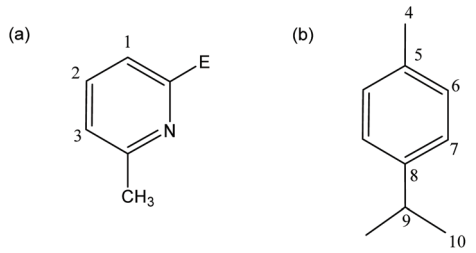

Fig. 12 The numbering schemes used for (a) the 6-Me-2-py groups and (b) the cymene groups in **9a** and **9b**.

Synthesis of new compounds

Synthesis of 1a-O. Inside a N_2 filled glovebox a Schlenk tube was charged with **1a** (900 mg, 2.562 mmol) and transferred to a Schlenk line. 50 ml of THF and 324 μl H_2O_2 (30% w/v, 1.1 equiv., 2.818 mmol) were added. The resulting clear solution was stirred for 5 days at room temperature. The solvent was removed *in vacuo* and the resulting solid mixture was washed with 20 ml of hexane. The product was dried *in vacuo* to yield **1a**-O as a colourless powder (675 mg, 1.838 mmol, 72%). A solution of 20 mg of the product in 0.5 ml of thf was transferred to a crystallization tube and layered with 10 ml of *n*-pentane. After 10 days at room temperature colourless crystals formed which were suitable for X-ray crystallography. ^{1}H NMR (25 °C, $CDCl_3$, 399.60 MHz): δ [ppm] = 7.95 (d, $^3J_{HH}$ = 6.7 Hz, 1H, H-1), 7.66 (t, $^3J_{HH}$ = 6.8 Hz, 3H, H-2), 7.22 (d, $^3J_{HH}$ = 7.1 Hz, 3H, H-3), 2.54 (s, 9H, CH_3); ^{13}C{^{1}H} NMR (25 °C, $CDCl_3$, 100.48 MHz): δ [ppm] = 159.99 (C_q, **C**–CH_3), 156.80 (C_q, As–**C**), 136.37 (C–H, C-2), 125.63 (C–H, C-1), 125.54 (C–H, C-3), 24.51 (C–**C**H_3); elemental analysis (%): calcd for **1a**-O, C 58.9% H 4.9% N 11.4%; found, C 58.2% H 4.9% N 11.1%; IR: ν [cm^{-1}] = 3106 (w), 3075 (w), 3035 (w), 3004 (w), 2962 (w), 2923 (w), 2854 (w), 2732 (w), 1770 (w), 1582 (s), 1551 (s), 1443 (s), 1377 (w), 1259 (s), 1176 (w), 1163 (w), 1135 (w), 1082 (s), 1034 (s), 981 (s), 902 (s), 845 (w), 802 (s), 784 (s), 733 (s), 706 (w), 667 (w), 557 (s), 545 (s), 533 (s), 422 (w).

Synthesis of 2. Inside a N_2 filled glovebox a Schlenk tube was charged with **1a**-O (100 mg, 0.272 mmol) and Tetrakis (acetonitrile)copper(I) hexafluorophosphate (101 mg, 0.272 mmol) and transferred to a Schlenk line. 20 ml of acetonitrile was added. The resulting yellow solution was stirred overnight at room temperature. A colourless precipitate formed overnight and was removed by filtration. The clear yellow filtrate was concentrated *in vacuo* until the precipitation of a yellow solid was observed which was dissolved into solution by gentle heating. Storage at −20 °C yielded a yellow crystalline solid which was washed twice with hexane to yield **2** as yellow crystals suitable for single crystal X-ray diffraction (52 mg, 0.0843 mmol, 31%). ^{1}H NMR (238 K, $CDCl_3$, 500.20 MHz): δ [ppm] = 8.05 (d, $^3J_{HH}$ = 7.0 Hz, 3H, H-1), 8.00 (t, $^3J_{HH}$ = 7.6 Hz, 3H, H-2), 7.58 (d, $^3J_{HH}$ = 7.7 Hz, 3H, H-3), 2.81 (s, 9H, CH_3), 1.99 (s, 3H, Cu–NC–CH_3); ^{1}H NMR (335 K, $CDCl_3$, 500.20 MHz): δ [ppm] = 8.08 (3H), 8.03 (3H), 7.60 (3H), 2.83 (s, 9H, CH_3), 1.99 (s, 3H, Cu–NC–CH_3); elemental analysis (%): calcd for **2**, C 38.9% H 3.4% N 9.1%; found, C 38.5% H 3.3% N

9.1%; IR: ν [cm^{-1}] = 3067 (w), 2940 (w), 2308 (w), 2273 (w), 2155 (w), 2030 (w), 2008 (w), 1986 (w), 1936 (w), 1731 (w), 1589 (w), 1550 (w), 1446 (w), 1384 (w), 1368 (w), 1257 (w), 1173 (w), 1165 (w), 1132 (w), 1092 (w), 1038 (w), 1002 (w), 927 (w), 878 (w), 834 (s), 796 (s), 734 (w), 675 (w), 556 (s), 481 (w), 449 (w), 430 (w).

Synthesis of 3. Inside a N_2 filled glovebox a Schlenk tube was charged with **1a** (50 mg, 0.142 mmol) and silver trifluoroacetate (39 mg, 0.178 mmol) and transferred to a Schlenk line. 20 ml of dry acetonitrile was added. The solution was stirred overnight at room temperature. A colourless precipitate was removed by filtration. The filtrate was concentrated *in vacuo* and then layered with 15 ml of diethyl ether. After 3 days at room temperature colourless crystals formed which were suitable for X-ray crystallography (34 mg, 0.0135 mmol, 38%, based on full occupancy of the Ag sites). ^{1}H NMR (25 °C, CD_3CN, 500.05 MHz): δ [ppm] = 7.77 (s, 1H, H–Ar), 7.27 (s, 1H, H–Ar), 6.98 (s, 1H, H–Ar), 2.24 (s, 3H, CH_3); ^{13}C NMR shows multiple overlapping signals; elemental analysis (%): calcd for **3** (based on full occupancy of the Ag sites), C 39.3% H 2.9% N 6.7%; found, C 40.5% H 2.9% N 7.5%; IR: ν [cm^{-1}] = 3416 (w), 3058 (w), 2918 (w), 1686 (s), 1591 (w), 1550 (w), 1448 (s), 1389 (w), 1197 (s), 1156 (s), 1108 (s), 1038 (w), 1003 (s), 847 (w), 816 (w), 795 (s), 784 (s), 728 (w), 714 (s), 674 (w), 596 (w), 556 (w), 541 (w), 516 (w), 412 (w).

Synthesis of 4. Inside a N_2 filled glovebox a Schlenk tube was charged with **4** (50 mg, 0.136 mmol) and silver trifluoroacetate (30 mg, 0.136 mmol) **1a**-O and transferred to a Schlenk line. 10 ml of acetonitrile was added. The resulting clear solution was stirred overnight at room temperature. The clear solution was concentrated *in vacuo* until the precipitation of a white solid was observed which was dissolved into solution by gentle heating. Storage at −20 °C yielded colourless crystals suitable for X-ray crystallography (16 mg, 0.0279 mmol, 20%). ^{1}H NMR (25 °C, CD_3CN, 500.20 MHz): δ [ppm] = 8.06 (d, $^3J_{HH}$ = 7.5 Hz, 3H, H-1), 7.94 (t, $^3J_{HH}$ = 7.8 Hz, 3H, H-2), 7.55 (d, $^3J_{HH}$ = 7.9 Hz, 3H, H-3), 2.74 (s, 9H, CH_3); ^{13}C{^{1}H} NMR (25 °C, CD_3CN, 125.78 MHz): δ [ppm] = 160.93 (C_q, **C**–CH_3), 157.14 (C_q, **C**–As), 138.85 (C–H, C-2), 127.13 (C–H, C-1), 125.24 (C–H, C-3), 24.82 (C–**CH_3**). (The assignment of the two C_q carbons was determined from the HMBC.); elemental analysis (%): calcd for **4**, C 40.8% H 3.1% N 7.1%; found, C 39.5% H 2.8% N 5.7%; IR: ν [cm^{-1}] = 3063 (w), 3009 (w), 2980 (w), 2962 (w), 2929 (w), 2301 (w), 1704 (w), 1668 (s), 1589 (s), 1551 (w), 1445 (s), 1418 (w), 1383 (w), 1254 (w), 1198 (s), 1177 (s), 1132 (s), 1089 (w), 1038 (w), 996 (w), 916 (s), 834 (w), 795 (s), 732 (w), 721 (s), 672 (w), 597 (w), 555 (w), 520 (w), 454 (w), 406 (w).

Synthesis of 5. Inside a N_2 filled glovebox a Schlenk tube was charged with **1a** (200 mg, 0.569 mmol) and cobalt(II) bromide (124 mg, 0.569 mmol) and transferred to a Schlenk line. 20 ml of acetonitrile was added. The resulting dark blue solution was stirred overnight at room temperature. Dark blue crystals formed overnight. Storage at −20 °C yielded **5** as blue crystals suitable for single crystal X-ray diffraction (88 mg, 0.154 mmol, 27%). ^{1}H NMR (25 °C, CD_3CN, 500.12 MHz): δ [ppm] = 49.63, 37.10, 12.69, 7.17; elemental analysis (%): calcd for **5**, C 37.9% H 3.2% N 7.4%; found, C 37.8% H 3.1% N 7.2%; IR: ν [cm^{-1}] = 3066 (w), 3049 (w), 2989 (w), 2923 (w), 1588 (s), 1578 (s), 1551 (s), 1435 (s), 1373 (s), 1307 (s), 1231 (s), 1186 (s), 1169 (s), 1123 (s), 1095 (s), 1014 (s), 990 (s), 984 (s), 841 (w), 809 (s), 790 (s), 771 (s), 737 (s), 730 (s), 682 (w), 660 (w), 561 (w), 545 (s), 426 (s), 414 (s).

Synthesis of 6. Inside a N_2 filled glovebox a Schlenk tube was charged with **1a** (200 mg, 0.569 mmol) and nickel(II) bromide (124 mg, 0.569 mmol) and transferred to a Schlenk line. 20 ml of acetonitrile was added. The resulting clear green solution was stirred overnight at room temperature. A colourless precipitate formed overnight and was removed by filtration. The clear green filtrate was stored for 5 days at −20 °C and yielded **6** as purple crystals suitable for single crystal X-ray diffraction (70 mg, 0.123 mmol, 21.6%). Elemental analysis (%): calcd for **6**, C 37.9% H 3.2% N 7.4%; found, C 37.7% H 3.1% N 7.5%; IR: ν [cm^{-1}] = 3604 (w), 3344 (w), 3065 (w), 3050 (w), 3002 (w), 2922 (w), 2678 (w), 2097 (w), 2004 (w), 1912 (w), 1777 (w), 1706 (w), 1625 (w), 1590 (s), 1578 (s), 1552 (s), 1436 (s), 1371 (s), 1253 (w), 1245 (w), 1227 (w), 1187 (w), 1170 (w), 1133 (w), 1124 (w), 1100 (w), 1091 (w), 1018 (s), 994 (w), 975 (w), 914 (w), 842 (w), 809 (s), 790 (s), 772 (s), 731 (w), 684 (w), 661 (w), 562 (w), 545 (w), 448 (w), 428 (w), 415 (s).

Synthesis of 7. Inside a N_2 filled glovebox a Schlenk tube was charged with **1a**-O (150 mg, 0.408 mmol) and cobalt bromide (89 mg, 0.408 mmol) and transferred to a Schlenk line. 20 ml of acetonitrile was added. The resulting blue solution was stirred overnight at room temperature. The clear blue solution was concentrated *in vacuo* until the precipitation of a blue solid was observed which was dissolved into solution by gentle heating. Storage at −20 °C yielded blue crystals suitable for X-ray crystallography (188 mg, 0.150 mmol, 74%).^{1}H NMR (25 °C, CD_3CN, 500.12 MHz): δ [ppm] = 34.02, 28.14, 13.43, 11.10, 7.42, 6.57, 3.67, −1.54, −3.98; elemental analysis (%): calcd for **7**·CH_3CN, C 37.6% H 3.2% N 8.0%; found, C 37.5% H 3.0% N 7.9%; IR: ν [cm^{-1}] = 3371 (w), 3050 (w), 2988 (w), 2957 (w), 2922 (w), 2306 (w), 2279 (w), 2248 (w), 2026 (w), 2003 (w), 1914 (w), 1584 (w), 1549 (w), 1443 (s), 1389 (w), 1375 (w), 1308 (w), 1248 (w), 1232 (w), 1170 (w), 1129 (w), 1089 (w), 1036 (w), 983 (w), 914 (w), 858 (w), 829 (s), 790 (s), 774 (w), 728 (w), 674 (w), 543 (w), 448 (s), 424 (w).

Synthesis of 8. Inside a N_2 filled glovebox a Schlenk tube was charged with **1a**-O (150 mg, 0.408 mmol) and nickel(II) bromide (89 mg, 0.408 mmol) and transferred to a Schlenk line. 20 ml of acetonitrile was added. The resulting pale orange solution was stirred overnight at room temperature. A red solution with a small amount of brown precipitate formed overnight and was removed by filtration. The clear red filtrate was concentrated *in vacuo* until the precipitation of a yellow solid was observed which was dissolved into solution by gentle heating. Storage at −20 °C yielded a yellow crystalline solid which was washed twice with hexane to yield **8** as yellow crystals (7 mg, 0.010 mmol, 2%). 0.5 ml of the solution was transferred to a crystallization tube and layered with 10 ml of Et_2O. After 3 days at room temperature yellow crystals formed which were suitable for X-ray crystallography. Elemental analysis (%): calcd for **8**·CH_2Cl_2, C 34.0% H 3.0% N 6.3%; found, C 34.8% H

2.9% N 6.6%. IR: ν [cm^{-1}] = 3351 (w), 3281 (w), 3050 (w), 3006 (w), 2951 (w), 2921 (w), 2025 (w), 1910 (w), 1748 (w), 1705 (w), 1586 (s), 1547 (s), 1443 (s), 1402 (w), 1378 (w), 1335 (w), 1249 (w), 1182 (w), 1170 (w), 1133 (w), 1104 (w), 1085 (w), 1039 (w), 1005 (w), 993 (w), 860 (s), 830 (s), 789 (s), 761 (s), 729 (s), 674 (w), 554 (s), 526 (w), 455 (s), 423 (w).

Synthesis of 9a. Inside a N_2 filled glovebox a Schlenk tube was charged with **1a** (34 mg, 0.0968 mmol) and dichloro(*p*-cymene)ruthenium(II) dimer (30 mg, 0.0484 mmol) and transferred to a Schlenk line. 1 ml of dichloromethane was added. The resulting red solution was stirred for 10 minutes at room temperature. The solution was layered with approximately 10 ml of *n*-pentane. After 3 days at room temperature red crystals formed which were suitable for X-ray crystallography (42 mg, 0.0639 mmol, 66%); ^{1}H NMR (25 °C, CD_2Cl_2, 500.20 MHz): δ [ppm] = 7.66 (d, $^3J_{HH}$ = 7.7 Hz, 3H, H-1), 7.54 (t, $^3J_{HH}$ = 7.7 Hz, 3H, H-2), 7.18 (d, $^3J_{HH}$ = 7.7 Hz, 3H, H-3), 5.85 (d, $^3J_{HH}$ = 5.9 Hz, 2H, H-6), 5.68 (d, $^3J_{HH}$ = 5.9 Hz, 2H, H-7), 2.71 (sept, $^3J_{HH}$ = 6.9 Hz, 1H, H-9), 2.54 (s, 9H, C–**CH$_3$** of 6-Me-2-py group), 1.94 (s, 3H, H-4), 1.06 (d, $^3J_{HH}$ = 6.9 Hz, 6H, H-10). ^{13}C{^{1}H} NMR (25 °C, CD_2Cl_2, 125.78 MHz): δ [ppm] = 158.54 (C_q, **C**–As), 158.37 (C_q, **C**–**CH$_3$** of 6-Me-2-py group), 135.19 (C–H, C-2), 128.45 (C–H, C-1), 123.38 (C–H, C-3), 106.60 (C_q, C-8), 94.53 (C_q, C-5), 86.87 (C–H, C-6), 82.04 (C–H, C-7), 30.13 (C–H, C-19, 24.04 (CH_3, C–**CH$_3$** of 6-Me-2-py group), 21.44 (CH_3, C-10), 17.15 (CH_3, C-4); elemental analysis (%): calcd for **9a**, C 51.2% H 4.9% N 6.4%; found, C 51.1% H 4.8% N 6.3%; IR: ν [cm^{-1}] = 3037 (w), 2962 (w), 2921 (w), 2866 (w), 1579 (s), 1555 (s), 1496 (w), 1469 (w), 1438 (s), 1389 (w), 1375 (w), 1361 (w), 1327 (w), 1265 (w), 1248 (w), 1169 (w), 1120 (w), 1085 (w), 1060 (w), 1034 (w), 987 (w), 924 (w), 890 (w), 874 (w), 799 (s), 784 (w), 775 (s), 731 (s), 702 (w), 668 (w), 633 (w), 569 (w), 555 (w), 548 (w), 517 (w), 451 (w), 426 (w).

Synthesis of 9b. Inside a N_2 filled glovebox a Schlenk tube was charged with ligand **1b** (39 mg, 0.0980 mmol) and dichloro(*p*-cymene)ruthenium(II) dimer (30 mg, 0.049 mmol) and transferred to a Schlenk line. 1 ml of dichloromethane was added. The resulting red solution was stirred for 10 minutes at room temperature. The solution was layered with approximately 10 ml of *n*-pentane. After 3 days at room temperature red crystals formed which were suitable for X-ray crystallography (44 mg, 0.0625 mmol, 64%); ^{1}H NMR (25 °C, CD_2Cl_2, 500.20 MHz): δ [ppm] = 7.77 (d, $^3J_{HH}$ = 7.6 Hz, 3H, H-1), 7.49 (t, $^3J_{HH}$ = 7.7 Hz, 3H, H-2), 7.14 (d, $^3J_{HH}$ = 7.7 Hz, 3H, H-3), 6.08 (d, $^3J_{HH}$ = 6.0 Hz, 2H, H-6), 6.00 (d, $^3J_{HH}$ = 6.0 Hz, 2H, H-7), 2.81 (sept, $^3J_{HH}$ = 7.0 Hz, 1H, H-9), 2.56 (s, 9H, C–**CH$_3$** of 6-Me-2-py group), 2.06 (s, 3H, H-4), 1.16 (d, $^3J_{HH}$ = 7.0 Hz, 6H, H-10); ^{13}C{^{1}H} NMR (25 °C, CD_2Cl_2, 125.78 MHz): δ [ppm] = 160.34 (C_q, C–As), 159.13 (C_q, **C**–CH_3), 135.14 (C–H, C-2), 130.38 (C–H, C-1), 123.49 (C–H, C-3), 105.22 (C_q, C-8), 95.30 (C_q, C-5), 84.67 (C–H, C-6), 81.54 (C–H, C-7), 30.40 (C–H, C-9), 24.12 (CH_3, C–**CH$_3$** of 6-Me-2-py group), 21.60 (CH_3, C-10), 17.77 (CH_3, C-4); elemental analysis (%): calcd for **9b**, C 47.8% H 4.6% N 6.0%; found, C 48.5% H 5.1% N 5.7%; IR: ν [cm^{-1}] = 3066 (w), 3046 (w), 2956 (w), 2919 (w), 2868 (w), 2127 (w), 2121 (w), 2097 (w), 2088 (w), 1615 (w), 1576 (s), 1550 (s), 1504 (w), 1464 (w), 1435 (s), 1385 (w), 1370 (w), 1322 (w), 1246 (w), 1219 (w), 1200 (w), 1169 (s), 1118 (w), 1081 (s), 1056 (w), 1033 (w), 988 (s), 890 (w), 871 (w), 840 (w), 786 (s), 742 (w), 730 (w), 692 (w), 669 (w), 658 (w), 548 (w), 539 (s), 525 (w), 517 (w), 448 (w), 423 (w), 410 (w).

Synthesis of 10a. Inside a N_2 filled glovebox a Schlenk tube was charged with **1a** (45 mg, 0.127 mmol) and *cis*–bis(benzonitrile)dichloroplatinum(II) (30 mg, 0.0635 mmol) and transferred to a Schlenk line. 1 ml of dichloromethane was added. The resulting yellow solution was stirred for 10 minutes at room temperature. The solution was layered with approximately 10 ml of *n*-pentane. After 3 days at room temperature yellow crystals formed which were suitable for X-ray crystallography (36 mg, 0.0372 mmol, 59%). ^{1}H NMR (25 °C, CD_2Cl_2, 500.20 MHz): δ [ppm] = 8.04 (d, $^3J_{HH}$ = 7.7 Hz, 3H, H-1), 7.50 (t, $^3J_{HH}$ = 7.7 Hz, 3H, H-2), 7.05 (d, $^3J_{HH}$ = 7.5 Hz, 3H, H-3), 2.27 (s, 9H, C–**CH$_3$**); ^{13}C{^{1}H} NMR (25 °C, $CDCl_3$, 125.78 MHz): δ [ppm] = 158.20 (C_q, **C**–CH_3), 156.29 (C_q, As–**C**), 135.42 (t, C-2), 127.77 (t, C-1), 123.64 (t, C-3), 23.59 (C–**CH$_3$**); elemental analysis (%): calcd for **10a**, C 44.6% H 3.8% N 8.7%; found, C 43.8% H 3.7% N 8.3%; IR: ν [cm^{-1}] = 3046 (w), 2960 (w), 2922 (w), 2103 (w), 1911 (w), 1813 (w), 1793 (w), 1679 (w), 1580 (s), 1553 (s), 1438 (s), 1374 (w), 1247 (w), 1168 (w), 1128 (w), 1089 (w), 1031 (w), 989 (w), 921 (w), 903 (w), 781 (s), 729 (s), 698 (w), 666 (w), 559 (w), 548 (s), 535 (w), 421 (w), 402 (s).

Synthesis of 10b. Inside a N_2 filled glovebox a Schlenk tube was charged with **1b** (51 mg, 0.127 mmol) and *cis*-bis(benzonitrile)dichloroplatinum(II) (30 mg, 0.0635 mmol) and transferred to a Schlenk line. 1 ml of dichloromethane was added. The resulting yellow solution was stirred for 10 minutes at room temperature. The solution was layered with approximately 10 ml of *n*-pentane. After 3 days at room temperature yellow crystals formed which were suitable for X-ray crystallography (21 mg, 0.0183 mmol, 29%). ^{1}H NMR (25 °C, CD_2Cl_2, 500.20 MHz): δ [ppm] = 7.99 (d, $^3J_{HH}$ = 7.5 Hz, 3H, H-1), 7.51 (t, $^3J_{HH}$ = 7.7 Hz, 3H, H-2), 7.03 (d, $^3J_{HH}$ = 7.5 Hz, 3H, H-3), 2.24 (s, 9H, CH_3); ^{13}C{^{1}H} NMR (25 °C, $CDCl_3$, 125.78 MHz): δ [ppm] = 159.10 (C_q, **C**–Me) 158.00 (C_q, Sb–C), 135.33 (C–H, C-2), 129.63 (C–H, C-1), 123.84 (C–H, C-3), 23.55 (C–**CH$_3$**); elemental analysis (%): calcd for **10b**, C 38.7% H 3.3% N 7.3%; found, C 39.4% H 3.4% N 7.4%; IR: ν [cm^{-1}] = 3048 (w), 2961 (w), 2924 (w), 2007 (w), 1977 (w), 1681 (w), 1622 (w), 1576 (s), 1549 (s), 1435 (s), 1389 (w), 1372 (w), 1272 (w), 1247 (w), 1168 (s), 1122 (w), 1083 (w), 1035 (w), 990 (w), 980 (w), 901 (w), 840 (w), 780 (s), 728 (s), 696 (w), 659 (w), 546 (w), 529 (w), 416 (w).

Conflicts of interest

There are no conflicts of interest.

Acknowledgements

We thank the Leverhulme Trust (Grant for DSW and RG-R), The Spanish Ministry of Science, Innovation and Universities

(MCIU) (grant for RG-R, project number PGC2018-096880-A-I00), the Spanish MINECO-AEI and The EU (ESF) for a Ramon y Cajal contract (RG-R, RYC-2015-19035) and the Cambridge Trust (Vice Chancellor Scholarship for AJP), The EPSRC and the Royal Dutch Shell co. Ltd. (I-Case studentship for RBJ, grant EP/R511870/1) and The University of Valladolid and Santander Bank (Fellowship for AG-R).

References

1 L. H. Gade and P. Hofmann, *Molecular Catalysts: Structure and Functional Design*, John Wiley & Sons, 2014.
2 I. Kuzu, I. Krummenacher, J. Meyer, F. Armbruster and F. Breher, *Dalton Trans.*, 2008, 5836–5865.
3 A. Caballero, M. M. Díaz-Requejo, M. R. Fructos, J. Urbano and P. J. Pérez, in *Ligand Design in Metal Chemistry*, John Wiley & Sons, Ltd, 2016, pp. 308–329.
4 S. Trofimenko, *Chem. Rev.*, 1972, **72**, 497–509.
5 S. Trofimenko, *Chem. Rev.*, 1993, **93**, 943–980.
6 H. R. Simmonds and D. S. Wright, *Chem. Commun.*, 2012, **48**, 8617–8624.
7 G. M. Pawar, J. B. Sheridan and F. Jäkle, *Eur. J. Inorg. Chem.*, 2016, **2016**, 2227–2235.
8 L. F. Szczepura, L. M. Witham and K. J. Takeuchi, *Coord. Chem. Rev.*, 1998, **174**, 5–32.
9 C. S. Alvarez, F. García, S. M. Humphrey, A. D. Hopkins, R. A. Kowenicki, M. McPartlin, R. A. Layfield, R. Raja, M. C. Rogers, A. D. Woods and D. S. Wright, *Chem. Commun.*, 2005, 198–200.
10 Á. García-Romero, A. J. Plajer, L. Álvarez-Miguel, A. D. Bond, D. S. Wright and R. García-Rodríguez, *Chem. – Eur. J.*, 2018, **24**, 17019–17026.
11 E. Yang, A. J. Plajer, Á. García-Romero, A. D. Bond, T. K. Ronson, C. M. Álvarez, R. García-Rodríguez, A. L. Colebatch and D. S. Wright, *Chem. – Eur. J.*, 2019, **25**, 14003.
12 A. J. Plajer, S. Kopf, A. L. Colebatch, A. D. Bond, D. S. Wright and R. García-Rodríguez, *Dalton Trans.*, 2019, **48**, 5692–5697.
13 M. A. Beswick, M. K. Davies, P. R. Raithby, A. Steiner and D. S. Wright, *Organometallics*, 1997, **16**, 1109–1110.
14 F. García, A. D. Hopkins, R. A. Kowenicki, M. McPartlin, M. C. Rogers and D. S. Wright, *Organometallics*, 2004, **23**, 3884–3890.
15 R. García-Rodríguez and D. S. Wright, *Dalton Trans.*, 2014, **43**, 14529–14532.
16 R. García-Rodríguez, S. Hanf, A. D. Bond and D. S. Wright, *Chem. Commun.*, 2017, **53**, 1225–1228.
17 A. J. Plajer, A. L. Colebatch, F. J. Rizzuto, P. Pröhm, A. D. Bond, R. García-Rodríguez and D. S. Wright, *Angew. Chem., Int. Ed.*, 2018, **57**, 6648–6652.
18 T. Gneuß, M. J. Leitl, L. H. Finger, N. Rau, H. Yersin and J. Sundermeyer, *Dalton Trans.*, 2015, **44**, 8506–8520.
19 A. Steiner and D. Stalke, *Organometallics*, 1995, **14**, 2422–2429.
20 G. B. Deacon and J. H. S. Green, *Spectrochim. Acta, Part A*, 1969, **25**, 355–364.
21 T. Osako, Y. Tachi, M. Taki, S. Fukuzumi and S. Itoh, *Inorg. Chem.*, 2001, **40**, 6604–6609.
22 R. T. Jonas and T. D. P. Stack, *Inorg. Chem.*, 1998, **37**, 6615–6629.
23 Y. Shimazaki, H. Yokoyama and O. Yamauchi, *Angew. Chem., Int. Ed.*, 1999, **38**, 2401–2403.
24 M. Kodera, Y. Kajita, Y. Tachi and K. Kano, *Inorg. Chem.*, 2003, **42**, 1193–1203.
25 A. V. Artem'ev, I. Y. Bagryanskaya, E. P. Doronina, P. M. Tolstoy, A. L. Gushchin, M. I. Rakhmanova, A. Y. Ivanov and A. O. Suturina, *Dalton Trans.*, 2017, **46**, 12425–12429.
26 M. Nardelli, C. Pelizzi, G. Pelizzi and P. Tarasconi, *Dalton Trans.*, 1985, 321; S. W. Ng, *Acta Crystallogr., Sect. E: Struct. Rep. Online*, 2012, **68**, m1537; G. A. Bowmaker, Effendy, R. D. Hart, J. D. Kildea, E. N. de Silva, B. W. Skelton and A. H. White, *Aust. J. Chem.*, 1997, **50**, 539; U. M. Tripathi, A. Bauer and H. Schmidbaur, *Dalton Trans.*, 1997, 2865; A. Bonardi, A. Cantoni, C. Pelizzi, G. Pelizzi and P. Tarasconi, *J. Organomet. Chem.*, 1991, **402**, 281; A. Cingolani, Effendy, J. V. Hanna, M. Pellei, C. Pettinari, C. Santini, B. W. Skelton and A. H. White, *Inorg. Chem.*, 2003, **42**, 4938.
27 A. V. Artem'ev, J. A. Eremina, E. V. Lider, O. V. Antonova, E. V. Vorontsova and I. Yu Bagryanskaya, *Polyhedron*, 2017, **138**, 218–224.
28 A. J. Plajer, A. L. Colebatch, M. Enders, Á. García-Romero, A. D. Bond, R. García-Rodríguez and D. S. Wright, *Dalton Trans.*, 2018, **47**, 7036–7043.
29 P. Espinet, R. Hernando, G. Iturbe, F. Villafañe, A. G. Orpen and I. Pascual, *Eur. J. Inorg. Chem.*, 2000, **2000**, 1031–1038.
30 Y.-R. Luo, *Comprehensive Handbook of Chemical Bond Energies*, CRC Press, 2007.
31 Á. García-Romero, A. J. Plajer, D. Miguel, D. S. Wright, A. D. Bond, C. M. Álvarez and R. García-Rodríguez, *Inorg. Chem.*, 2020, **59**, 7103.
32 R. Cini, C. Bellucci, G. Tamasi, M. Corsini, M. Fontani and P. Zanello, *Inorg. Chim. Acta*, 2002, **339**, 89–103.
33 J. H. Nelson, K. Y. Ghebreyessus, V. C. Cook, A. J. Edwards, W. Wielandt, S. B. Wild and A. C. Willis, *Organometallics*, 2002, **21**, 1727–1733.
34 S. Otto and M. H. Johansson, *Inorg. Chim. Acta*, 2002, **329**, 135–140.
35 O. F. Wendt, A. Scodinu and L. I. Elding, *Inorg. Chim. Acta*, 1998, **277**, 237–241.

